Sustainable Carbon Materials

https://doi.org/10.48130/scm-0026-0001

Original Research

Open Access

Rapid microwave synthesis of nitrogen-doped ultramicroporous coal-based carbon with enhanced CO_2 adsorption performance

Yulin Feng[1], Xiaoxiao Meng[1*], Jingyu Li[1], Naiyuan Xue[1], Wanjing Li[1], Miaoting Sun[1], Jiaxiang Chen[1], Xingxing Wang[2], Ruida Zhou[2], Wenjun Zhuang[2], Jihui Gao[1], Guangbo Zhao[1] and Wei Zhou[1*]

Received: 13 November 2025

Revised: 5 January 2026

Accepted: 7 January 2026

Published online: 4 February 2026

Abstract

Ningdong coal was used as the raw material to develop a synergistic 'pre-oxidation + microwave activation' strategy for the preparation of nitrogen/oxygen co-doped ultramicroporous coal-based activated carbons (ACs), for efficient CO_2 adsorption. By tuning the microwave power and pretreatment conditions, the microcrystalline structure, pore size distribution, and surface functional groups of the ACs were precisely controlled. The results show that pre-oxidation significantly enhances nitrogen retention and doping efficiency, forming CO_2-philic active sites dominated by pyridinic and pyrrolic nitrogen, with a maximum nitrogen content of 10.06 at.%. Meanwhile, a large number of ultramicropores (0.6–0.7 nm) were constructed, which effectively improved the CO_2 adsorption capacity and selectivity. The optimized sample achieved CO_2 uptake of 4.72 mmol·g^{-1} at 0 °C and 1 bar, and maintained 3.33 mmol·g^{-1} at 25 °C, with CO_2/N_2 selectivity greater than 50. This work provides theoretical guidance and a practical pathway for the structure–function co-regulation and carbon capture applications of low-cost coal-derived ACs.

Keywords: Coal-based activated carbon, Microwave heating, Nitrogen/oxygen co-doping, CO_2 adsorption, Ultramicropores

Highlights

- Coal-based activated carbon is rapidly synthesized by microwave heating within 10 min.
- A high fraction of ultramicropores (0.6–0.7 nm) is constructed for efficient CO_2 confinement.
- Pre-oxidation–induced oxygen substitution enables ultrahigh nitrogen doping up to 10.06 at.%.
- The optimized carbon exhibits a CO_2 uptake of 3.33 mmol·g^{-1} at 25 °C with high CO_2/N_2 selectivity.

Graphical abstract

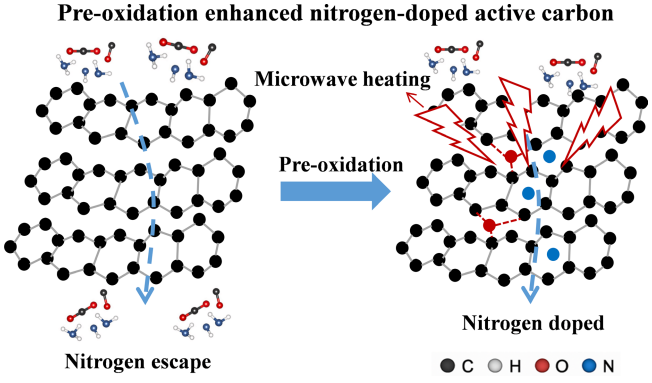

* Correspondence: Xiaoxiao Meng (mengxiaoxiao@hit.edu.cn); Wei Zhou (hitzhouw@hit.edu.cn)

Full list of author information is available at the end of the article.

https://doi.org/10.48130/scm-0026-0001

Introduction

With the continuous increase in global greenhouse gas emissions, carbon dioxide (CO_2) has become the primary contributor to global warming[1–3]. Therefore, developing efficient, low-energy, and scalable CO_2 capture technologies is critical for achieving carbon neutrality. Among various approaches, adsorption using carbon-based materials has attracted extensive attention owing to their high surface area, chemical stability, and structural tunability[4,5]. In particular, introducing heteroatoms such as nitrogen and oxygen into carbon frameworks has been widely demonstrated to enhance CO_2 affinity by increasing surface polarity, and Lewis basicity[6–9].

To date, most heteroatom-doped porous carbons are prepared via conventional tube-furnace heating combined with chemical activation. However, this strategy inherently relies on prolonged high-temperature treatment (> 700 °C), which inevitably causes severe volatilization of nitrogen- and oxygen-containing species below 600 °C, leading to low heteroatom retention and poor controllability of surface chemistry[10–12]. As a result, the nitrogen content of activated carbons produced by conventional heating typically remains below ~5 at.%, and further enhancement often requires excessive addition of nitrogen precursors at the expense of pore accessibility and adsorption efficiency[13].

Recent studies on heteroatom-doped biomass-derived carbons have emphasized the importance of synergistically optimizing narrow microporosity and surface functionality for CO_2 adsorption. For example, N/S-co-doped carbons derived from coconut shell exhibit enhanced CO_2 uptake due to the combined contribution of heteroatom-rich active sites and ultramicropores, although their synthesis still relies on conventional thermal routes with limited heteroatom utilization efficiency[14]. Similarly, boron-doped porous carbons prepared using metaborate activators demonstrate improved CO_2 affinity through electronic structure modulation, yet the high activation temperatures required still restrict precise control over dopant retention and spatial distribution[15,16]. These studies highlight that, despite notable progress, the fundamental challenge of simultaneously achieving efficient heteroatom incorporation, controlled pore evolution, and energy-efficient processing remains unresolved.

Microwave-assisted heating has recently emerged as a promising alternative due to its volumetric, selective, and rapid heating characteristics[17]. Unlike conventional external heating, microwave irradiation enables direct coupling between electromagnetic energy and carbon precursors, offering the potential to accelerate pore formation while suppressing excessive heteroatom loss. Nevertheless, most existing microwave-based studies focus primarily on rapid activation or morphology evolution, while the role of precursor pre-oxidation in regulating microwave energy coupling, heteroatom substitution pathways, and pore blockage effects has rarely been systematically explored.

In this work, a pre-oxidation–assisted microwave activation strategy is proposed for coal-derived carbon materials. Pre-oxidation introduces abundant oxygen-containing active sites that facilitate subsequent nitrogen substitution under microwave irradiation, thereby mitigating nitrogen loss and alleviating pore blockage induced by bulky nitrogen functionalities. As schematically illustrated in Fig. 1, this strategy fundamentally differs from both conventional tube-furnace activation and direct microwave activation of raw coal, enabling more efficient energy utilization, enhanced heteroatom retention, and improved accessibility of ultramicropores. This work thus provides new mechanistic insight into the pre-oxidation–microwave synergistic regulation of heteroatom doping and pore architecture, offering a viable pathway for the rational design of high-performance CO_2 adsorbents.

Herein, a scalable 'pre-oxidation + microwave activation' synergistic strategy is proposed to construct N/O co-doped ultramicroporous coal-based carbons. Benefiting from the high microwave absorption efficiency (> 90%) and volumetric heating properties, the production time of activated carbon was shortened to only 10 min. The oxygen-containing functional groups introduced by pre-oxidation facilitated oxygen-exchange reactions during microwave activation, thereby enhancing nitrogen incorporation.

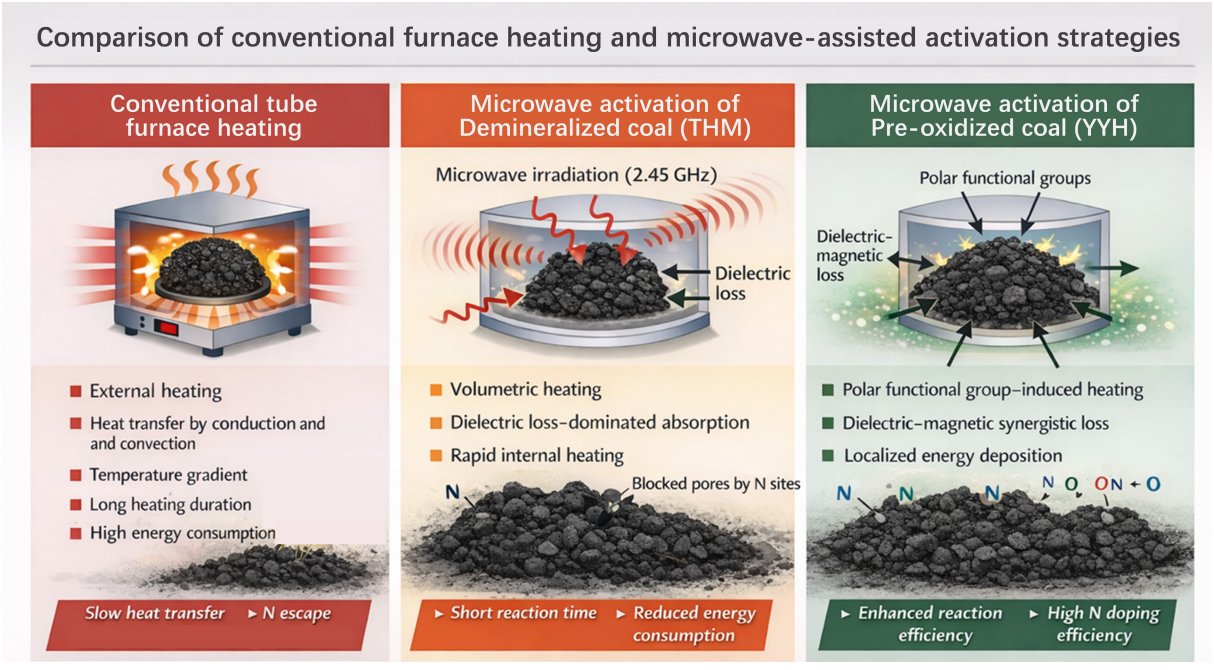

Fig. 1 Comparison of conventional furnace heating and microwave-assisted activation strategies.

Interestingly, the pre-oxidized samples exhibited an opposite trend to untreated coal—wherein nitrogen content increased with temperature, reaching a maximum of 10.06 at.%. The resulting materials exhibited superior CO_2 adsorption performance, achieving 4.72 mmol·g^{-1} at 0 °C and 1 bar, and maintaining 3.33 mmol·g^{-1} at 25 °C, along with excellent CO_2/N_2 selectivity (> 100). This work demonstrates that coupling thermochemical regulation with microwave-induced defect engineering enables simultaneous optimization of pore structure and surface functionality, offering a promising route for low-cost, high-efficiency coal-based adsorbents for carbon capture applications.

Materials and methods

Materials

Ningdong coal (proximate and ultimate analyses shown in Supplementary Table S1) with a particle size range of 0.2–0.425 mm (40–80 mesh) was subjected to acid-assisted demineralization using 15 wt% HCl, and 20 wt% HF solutions to remove inherent ash and inorganic impurities, yielding a purified carbon precursor referred to as de-ashed coal (THM). The obtained THM sample was subsequently pre-oxidized in a muffle furnace at 350 °C for 3 h under an air atmosphere, producing the pre-oxidized coal precursor (YYH). Thereafter, 2 g of the carbon precursor (THM or YYH) was homogeneously mixed with 4 g of KOH, and 2 g of melamine, and the resulting mixture was placed in a quartz tube for the microwave-assisted synthesis of activated carbon. For comparative testing, a control group was also prepared under different potassium hydroxide ratios, and without melamine doping.

Experimental system

As illustrated in Fig. 2, the microwave heating apparatus consisted of a single-mode resonant cavity (ZDM-3), a fixed-bed reactor, a microwave power meter (AV 2438 CB), an infrared (IR) temperature sensor, and an N_2 mass flow controller. The microwave power meter continuously monitored the incident and reflected power to calculate the absorbed microwave power and corresponding absorbed energy. Throughout the synthesis process, a constant N_2 flow rate of 100 mL·min^{-1} was maintained, with the microwave input power set to 200, 250, or 300 W, for a fixed irradiation duration of 10 min. After synthesis, the obtained activated carbons (ACs) were thoroughly washed with deionized water to remove residual potassium-containing species. The washing process was continued until the pH of the filtrate reached neutrality, after which the samples were dried to obtain the final activated carbon products. The resulting activated carbon samples were denoted as THM-200/250/300 W, and YYH-200/250/300 W, respectively.

Structural characterization

The porous structures of the samples were characterized by nitrogen adsorption–desorption isotherms using a 3H2000PM2 analyzer (Beishide Instrument Technology Co., Ltd, Beijing, China). The surface morphology of the activated carbons was examined by scanning electron microscopy (SEM, SU8010). Furthermore, the physical and chemical structures of the activated carbon samples were analyzed using electron paramagnetic resonance spectroscopy (EPR, MS5000), X-ray photoelectron spectroscopy (XPS, Thermo ESCALAB 250XI), X-ray diffraction (XRD, Rigaku SmartLab SE), Raman spectroscopy (Renishaw inVia Reflex, 532 nm excitation), and Fourier transform infrared spectroscopy (FTIR, Nicolet iZ10).

Adsorption characteristics of CO_2

The CO_2 adsorption performance of the samples was evaluated at 0 and 25 °C. For dynamic CO_2 adsorption measurements, a constant CO_2 feed flow rate of 2 mL·min^{-1} was applied at 25 °C to obtain the breakthrough curves. The dynamic adsorption characteristics were assessed based on the calculated adsorption capacity[18].

$$q_\tau = V\int_0^\tau (C_0 - C)\,\mathrm{d}t/m_{\mathrm{bed}} \tag{1}$$

In these calculations, C_0 (mg·m^{-3}) and C (mg·m^{-3}) represent the inlet and outlet CO_2 concentrations, respectively; t (min) denotes the adsorption time; q_t (g·g^{-1}) refers to the adsorption capacity; and V represents the gas flow rate. The CO_2 adsorption isotherms of 0.1 g samples were measured at 25 °C using a 3H2000 PM2 physical adsorption analyzer. The obtained isotherms were fitted using the Langmuir model (Eq. [2]), the Freundlich model (Eq. [3]), and the Sips model (Eq. [4]) to analyze the CO_2 adsorption behavior of the activated carbon[19].

$$q_e = q_m k_L p/(1 + k_L p) \tag{2}$$

$$q_e = k_F p^{1/n_F} \tag{3}$$

$$q_e = q_S k_S C^{1/n_S}/(1 + k_S C^{1/n_S}) \tag{4}$$

where, p (bar), k_L (bar^{-1}), q_s (mmol·g^{-1}), k_F ((bar^{-1})$^{1/nF}$, and n_F denote the equilibrium concentration, Langmuir constant, theoretical maximum adsorption capacity, Freundlich affinity constant, and the Freundlich

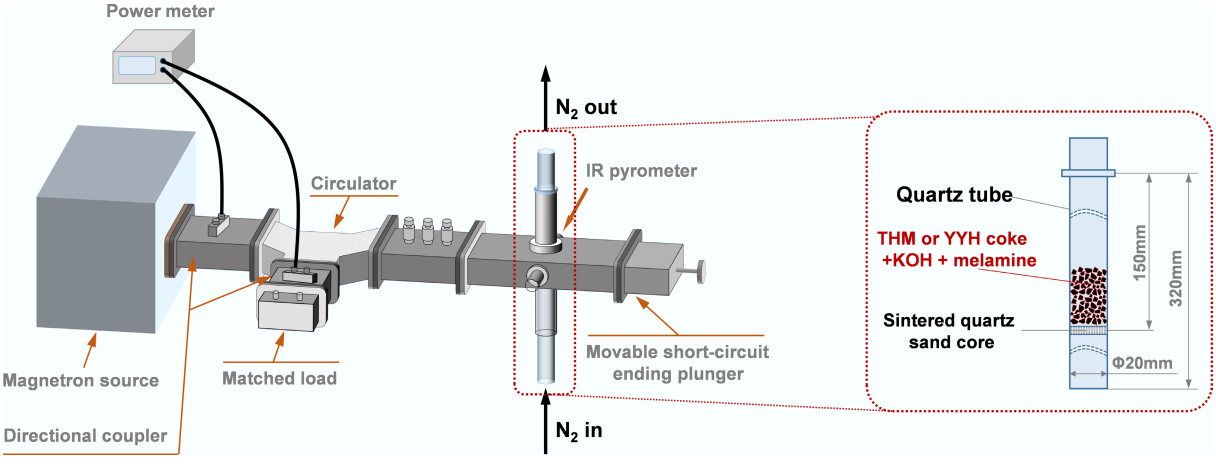

Fig. 2 Microwave heating system.

https://doi.org/10.48130/scm-0026-0001

constant, respectively. The k_S ($(bar^{-1})^{1/nS}$) and n_S denote the Sips constants.

Meanwhile, N_2 adsorption isotherms were also measured at 25 °C to investigate the selectivity of ACs using 0.1 g samples. The ideal adsorption solution theory (IAST) was used to calculate the adsorption selectivity of CO_2/N_2 (S_{ads})[20].

$$S_{ads} = q_1 p_2 / q_2 p_1 \quad (5)$$

where, q_1 and p_1 denote the adsorption volume and the partial pressure of CO_2, respectively. q_2 and p_2 represent the adsorption volume and the partial pressure of N_2, respectively. In this work, the fitted adsorption data obtained from the adsorption isotherm model for the IAST calculations, and the concentrations of CO_2 and N_2 are 85% and 15 %, respectively.

The isosteric heat of adsorption of CO_2 can be calculated as follows (Eq. [6]):

$$\ln(p2/p1) = -(\Delta H_{ads}/R)(1/T_2 - 1/T_1) \quad (6)$$

where, R denotes the universal gas constant, ΔHads denotes the isosteric heat of adsorption (kJ·mol^{-1}), T1 and T2 are 273 and 298 K, respectively.

Results and discussion

Microwave heating characteristics

Supplementary Figure S1 shows the dielectric constants of THM and YYH coal. In a 2.5 GHz microwave reactor, both coal samples exhibited a dielectric response and underwent microwave heating. In general, raw coal exhibits weak microwave absorption at low temperatures, whereas the introduction of KOH significantly enhances its microwave absorption capability[21]. Moreover, at elevated temperatures, the microwave absorption performance of coal is further improved due to increased electronic conduction and interfacial polarization effects.

Figure 2 presents the schematic diagram of the microwave heating system, and Fig. 3a illustrates the microwave heating characteristics of different carbon precursors under various input powers. As the input power increases from 200 to 300 W, the steady-state temperature gradually rises. Under identical input power conditions, the pre-oxidized coal precursor demonstrates a shorter response time, a higher heating rate, and a higher stable temperature than the de-ashed coal precursor. As shown in Fig. 3b, c, the microwave absorption power (MAP) rapidly reaches a steady value within 4 min, while the microwave absorption efficiency (MAE) stabilizes above 90%, indicating the fast-response characteristics and remarkable energy-saving potential of the microwave heating process. Furthermore, under the same input power, the total energy consumption, represented by the absorbed microwave energy, remains comparable across samples, with a typical value of approximately 45 kJ at 250 W, as presented in Fig. 3d.

Additionally, a thermal comparison was conducted between microwave heating and conventional tube furnace heating, as shown in Supplementary Fig. S2. Compared with conventional tube-furnace heating, microwave activation exhibits significantly higher energy efficiency. Under the conditions used in this study, conventional activation was conducted in a 7 kW tube furnace for 77.5 min, resulting in a total energy consumption of approximately 9.0 kWh.

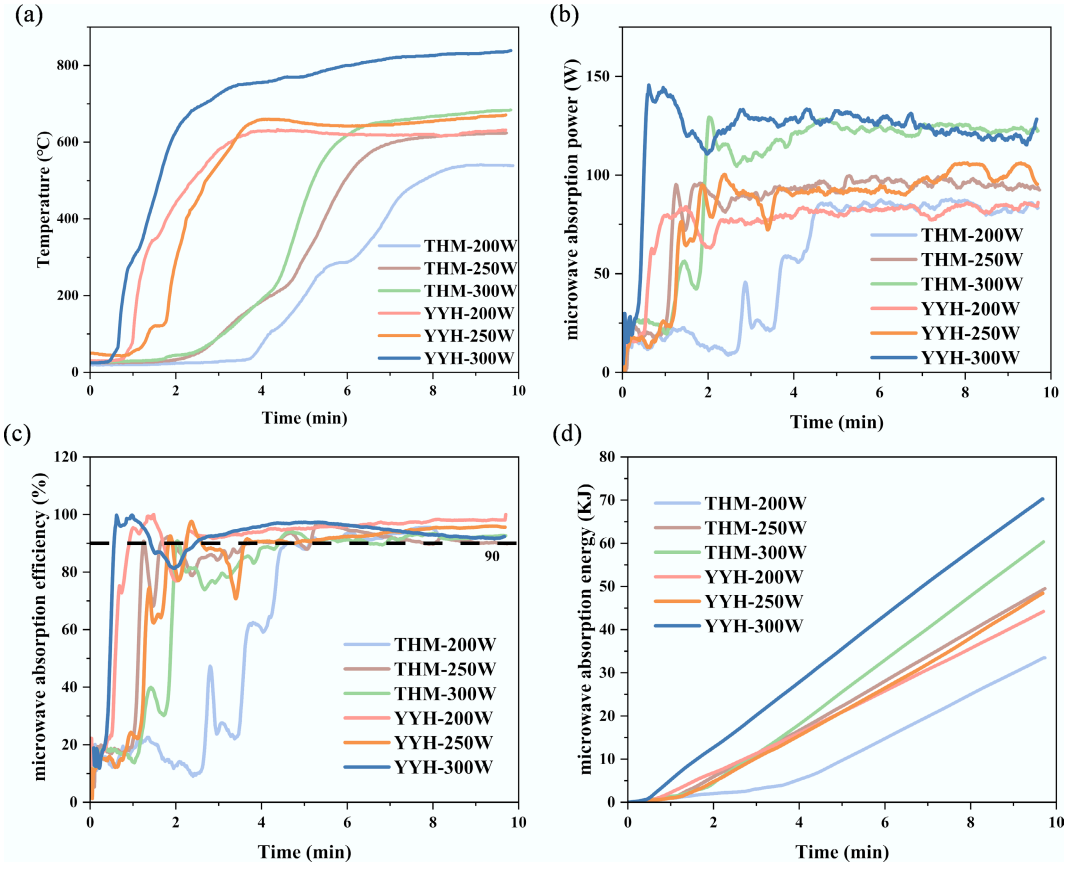

Fig. 3 Microwave heating system and heating characteristics: (**a**) temperature, (**b**) microwave absorption power, (**c**) microwave absorption efficiency, and (**d**) microwave absorption energy of different samples.

In contrast, microwave activation required only 250 W for 10 min, corresponding to an energy consumption of about 0.042 kWh, which is nearly two orders of magnitude lower than that of conventional heating. This demonstrates the superiority of microwave heating.

Pore structure characterization

The SEM images presented in Fig. 4a reveal the formation of abundant micron-sized pores and cracks on the carbon surface. These well-developed honeycomb-like pores and fissures are attributed to the expansion and release of volatile species (e.g., NH_3, H_2O) generated during microwave-induced thermal decomposition within the carbon matrix[22]. For the THM series (non-pre-oxidized coal), both the pore density and pore size increase significantly with rising microwave power. The surface of THM-200W exhibits sparse and relatively closed pores, whereas THM-250W displays pronounced honeycomb-like micropores interconnected by visible cracks. At THM-300W, a more developed and uniformly distributed hierarchical pore network is observed. A similar trend is evident in the YYH series (pre-oxidized coal). However, under the same microwave power, the YYH samples show more regular pore structures and thinner, more permeable pore walls. Notably, YYH-250W exhibits improved pore size uniformity and interconnectivity compared to THM-250W, indicating that the pre-oxidation treatment promotes more orderly pore evolution during microwave activation.

The six synthesized samples exhibited consistent and systematic pore structure evolution, as evidenced by both N_2 adsorption–desorption measurements and SEM observations. The corresponding adsorption–desorption isotherms (Fig. 4b) display a typical mixed Type I + Type IV behavior[23]. A sharp uptake at low relative pressure ($P/P_0 < 0.01$) indicates the presence of abundant micropores, while the appearance of a hysteresis loop in the medium-to-high pressure range signifies the existence of mesopores with diameters between 2 and 50 nm. The BET surface area increased progressively with higher microwave power and pre-oxidation treatment. Specifically, the surface area of THM-200W was 767 $m^2 \cdot g^{-1}$, which increased to 1,131 $m^2 \cdot g^{-1}$ for THM-300W. Meanwhile YYH-250W exhibited the highest value of 1,103 $m^2 \cdot g^{-1}$, slightly exceeding that of THM-250W (910 $m^2 \cdot g^{-1}$). The pore size distribution curves (Fig. 4c) show dominant peaks centered around 0.6–0.8 nm, characteristic of microporous structures. Notably, the peak positions for THM-250W and YYH-200W shift slightly toward smaller pore sizes, suggesting that the pre-oxidation treatment facilitates the generation of a greater abundance of ultramicropores within the carbon framework.

The pore volume distributions quantified by the NLDFT method (Fig. 4d) further corroborate these observations. In the THM series, the ultramicropore volume (< 0.7 nm) increased from 0.24 $cm^3 \cdot g^{-1}$ at 200 W to 0.35 $cm^3 \cdot g^{-1}$ at 300 W. For the YYH series, the ultramicropore volume reached 0.32 $cm^3 \cdot g^{-1}$ at 250 W, slightly higher than that of THM-250W (0.29 $cm^3 \cdot g^{-1}$). Meanwhile, both micropore (0.7–2 nm) and mesopore (> 2 nm) volumes exhibited a concurrent increase with rising microwave power. Although YYH-300W showed a slightly lower micropore volume (0.42 $cm^3 \cdot g^{-1}$) compared to THM-300W (0.46 $cm^3 \cdot g^{-1}$), it possessed a marginally higher mesopore volume (0.08 $cm^3 \cdot g^{-1}$), suggesting that pre-oxidation promotes a more balanced hierarchical pore structure conducive to gas adsorption and transport. Additionally, we performed aperture analysis on the representative sample (YYH-250W) using the DTF model, with results shown in Supplementary Fig. S3 and Supplementary Table S2. The results show a main peak at 0.6–0.7 nm, indicating that the sample is predominantly composed of ultramicroporous structures.

Accordingly, the obtained samples exhibited high microporosity. The micropore ratios of THM-200W, THM-250W, THM-300W, YYH-200W, YYH-250W, and YYH-300W were 86.62%, 91.27%, 89.94%, 84.76%, 82.99%, and 84.47%, respectively. Detailed pore structure parameters are summarized in Table 1.

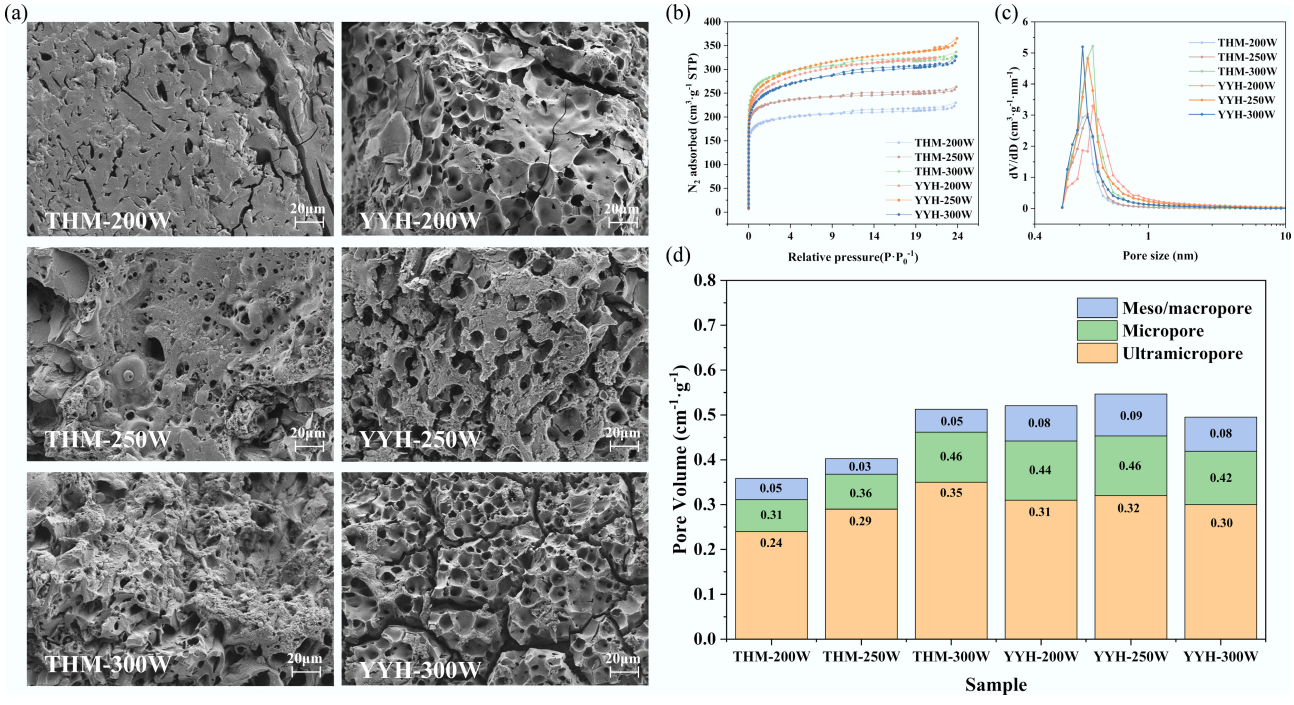

Fig. 4 The morphology and pore structure of samples: (**a**) SEM images, (**b**) N_2 adsorption–desorption isotherms, (**c**) NLDFT pore size distributions of samples, and (**d**) the micropore volume, meso/macropore volume, and ultramicro volume of samples.

https://doi.org/10.48130/scm-0026-0001

As shown in Fig. 4 and Table 1, pre-oxidation (YYH series) further optimized the pore structure under identical microwave powers, resulting in enhanced ultramicroporosity and improved overall pore connectivity. Such structural refinement facilitates gas diffusion and mass transfer during subsequent dynamic adsorption processes. The synergistic effect of microwave power and pre-oxidation markedly promotes the development of a well-defined hierarchical pore architecture in the coal-based activated carbons, thereby providing an efficient pore framework for high-performance CO_2 capture.

Simultaneously, throughout the entire activation process, factors such as varying KOH ratios and the inclusion or exclusion of melamine addition significantly influenced the results, in addition to microwave power. Therefore, we supplemented the above comparative experiments with results presented in Supplementary Figs S4, S5, and Supplementary Table S3.

Consequently, we ultimately concluded that the optimized conditions were coal to KOH ratio of 1:2 and the addition of melamine. The yields of activated carbon prepared at different power levels are shown in Supplementary Table S4, with values ranging from 41% to 55%. Moreover, as the microwave power increases, the yield decreases, and the yield of pre-oxidized coal is higher than that of delignified coal. This high yield demonstrates the potential for microwave-assisted carbon production in industrial applications.

Defects and surface functional groups characterization

Furthermore, the physicochemical structural characteristics of the synthesized activated carbons were systematically investigated to elucidate their structural evolution. Raman spectroscopy, a powerful technique for probing the degree of ordering and defect distribution in carbon materials, was employed to reveal the structural variations of sp^2-hybridized carbon frameworks. As shown in Fig. 5a, all samples exhibit the characteristic dual-band Raman features: the D band (~1,350 cm^{-1}), associated with disordered carbon (such as edge defects, lattice imperfections, or sp^3-hybridized structures), and the G band (~1,580 cm^{-1}), corresponding to the in-plane vibrations of graphitic sp^2 carbon atoms[24]. With the increase of microwave power from 200 to 300 W, the intensity of the D band becomes significantly stronger while that of the G band weakens, indicating that the higher energy density of microwave irradiation promotes more intense thermal decomposition reactions, leading to the generation of additional structural defects and a decrease in the overall graphitic order. This trend demonstrates that microwave irradiation not only accelerates the carbonization process but also plays a crucial role in tailoring the microstructural organization of the carbon framework.

As shown in Fig. 5b and Supplementary Fig. S6, the fitted spectra of the THM and YYH samples further elucidate the complex structural composition within the carbon materials. Specifically, the five sub-bands correspond to graphitic ordered carbon (G band), edge-defect carbon (D1), surface impurity-related carbon (D2), amorphous carbon (D3), and oxygen-containing functionalized carbon structures (D4)[25]. With increasing microwave power, the THM series exhibits a pronounced enhancement in the D1 and D3 bands, accompanied by a gradual attenuation of the G band, indicating that high-energy microwave irradiation induces significant structural disordering.

In contrast, the YYH series (pre-oxidized samples) displays stronger D1, D3, and D4 features under identical power levels, most notably in YYH-300W, suggesting that pre-oxidation promotes structural activation, amorphous carbon enrichment, and the formation of edge-related sites. Although increased disorder disrupts the graphitic ordering to some extent, it simultaneously introduces a higher density of active sites and surface defects, which can exert a favorable influence on CO_2 adsorption[26]. Moderate structural disorder enhances gas affinity and diffusion kinetics, thereby improving both adsorption capacity and dynamic performance. However, excessive defect generation or over-disordering may lead to pore collapse and surface area reduction, ultimately hindering adsorption efficiency. Therefore, the controlled regulation of microwave power and pre-oxidation conditions to achieve a state of moderate disorder in the carbon structure is crucial for optimizing CO_2 adsorption performance.

For the Raman spectra, the intensity ratio of the D1 band to the G band (I_{D1}/I_G) is commonly employed to evaluate the degree of disorder or defect density in activated carbons, as shown in Fig. 5c[27]. Compared with the non-pre-oxidized THM series, the YYH series (pre-oxidized) exhibits higher I_{D1}/I_G ratios under identical microwave power conditions, indicating that pre-oxidation further disrupts the graphitic framework and enhances the structural disorder of the carbon materials. Notably, molecular dynamics studies have demonstrated that an increased defect concentration facilitates heteroatom doping, which in turn contributes to the stabilization of the carbon framework[28]. Therefore, the high defect density induced by microwave irradiation provides a favorable environment for subsequent heteroatoms incorporation.

Figure 5d presents the EPR responses of the samples under different microwave powers. The results indicate that, with increasing microwave power, the peak intensity of the EPR signals for both the THM and YYH series gradually decreases, suggesting that some electron defects undergo reconstruction or 'healing' under high-energy microwave irradiation, leading to a more stabilized carbon framework and reduced defect activity[29]. Moreover, at 250 and 300 W, the $I_{peak,EPR}$ of the YYH samples is notably higher than that of the corresponding THM samples, implying that pre-oxidation introduces additional initial radical sites, which are more responsive under microwave excitation. This effect is particularly pronounced at medium-to-high power levels, indicating that the pre-oxidation treatment promotes defect formation in the carbon matrix.

Table 1 Parameters of pore structure for ACs

Sample	S_{BET} ($m^2 \cdot g^{-1}$)	V_{micro} ($cm^3 \cdot g^{-1}$)	V_{total} ($cm^3 \cdot g^{-1}$)	V_{micro}/V_{total} (%)	$V_{ultramicro}$ ($cm^3 \cdot g^{-1}$)	$V_{ultramicro}/V_{total}$ (%)	H–K average pore size (nm)
THM-200	767	0.31	0.36	86.62	0.24	66.61	0.70
THM-250	910	0.36	0.40	91.27	0.29	71.74	0.67
THM-300	1131	0.46	0.51	89.94	0.35	68.01	0.70
YYH-200	1057	0.44	0.52	84.76	0.31	59.27	0.70
YYH-250	1103	0.46	0.55	82.99	0.32	58.73	0.70
YYH-300	1008	0.42	0.49	84.47	0.30	60.31	0.69

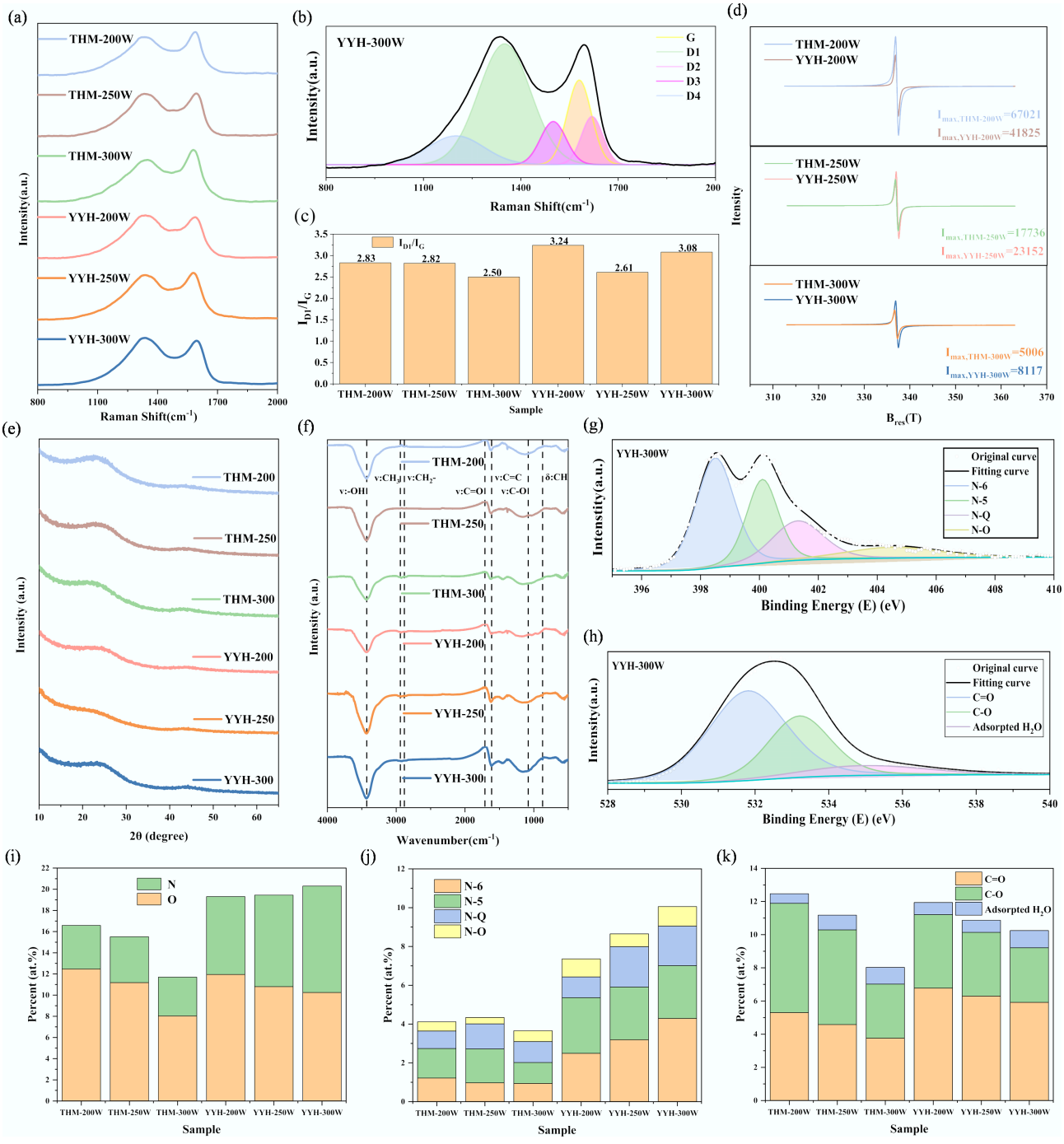

Fig. 5 Physicochemical structure characterizations: (**a**) Raman spectrum, (**b**) Raman spectrum fitted into five bands of CH-0, (**c**) I_{D1}/I_G, (**d**) EPR spectroscopy, (**e**) XRD spectrum, (**f**) FTIR spectrum, (**g**) deconvoluted N1s spectrum of YYH-300W, (**h**) deconvoluted O1s spectrum of YYH-300W, (**i**) nitrogen and oxygen content of samples, (**j**) nitrogen functional groups distributions, and (**k**) oxygen functional groups distributions.

XRD is widely used in the carbon materials field to evaluate both the stacking order of carbon layers and the variations in graphite microcrystal size, interlayer spacing, and overall carbon framework ordering[30]. In this study, as shown in Fig. 5e, all samples exhibit two characteristic diffraction peaks at approximately 23° and 43°, corresponding to the (002) and (100) planes of the carbon materials, respectively. The (002) plane reflects the stacking structure of graphite layers and serves as an important indicator of graphitization degree, whereas the (100) plane represents the in-plane atomic arrangement of graphite crystallites[31]. The broad and weak nature of the (002) diffraction peaks across all samples indicates that the materials are predominantly amorphous carbon with only minor, low-degree graphitized microcrystalline structures. This observation suggests that under the employed microwave treatment conditions, although carbonization and structural reorganization occur, highly ordered graphite structures are not formed, and the carbon framework remains largely disordered. These findings are consistent with the Raman and EPR analyses, collectively revealing the structural

https://doi.org/10.48130/scm-0026-0001

evolution of the carbon materials under different processing conditions.

The microcrystalline structural parameters, including L_a, L_c, and d_{002}, were further calculated using the Bragg and Scherrer equations to quantify the lateral size, vertical stacking height, and interlayer spacing of the carbon layers, thereby assessing changes in structural ordering of the carbon materials[32]. As summarized in Table 2, within the THM series, increasing the microwave power from 200 to 300 W led to a decrease in d_{002} from 0.38 to 0.35 nm, followed by a slight rebound, while L_a decreased from 4.43 to 3.40 nm. This indicates that moderate microwave power promotes denser stacking of carbon layers and enhances structural ordering, whereas excessively high power may cause partial ablation or disturbance of the layers, resulting in a slight lateral expansion. The L_c values remained relatively constant (0.94–1.00 nm), reflecting stable layer stacking numbers. In contrast, the pre-oxidized YYH series exhibited overall larger d_{002} values (up to 0.39 nm for YYH-250W), and smaller L_a values (minimum of 3.06 nm for YYH-250W), indicating that pre-oxidation introduces oxygen-containing functional groups that disrupt π–π stacking between carbon layers, weaken the regularity of microcrystalline structures, and further promote structural disorder.

These XRD trends are consistent with the Raman spectroscopy results, specifically, the increase in the I_{D1}/I_G ratio, and the enhanced defect concentration observed in EPR analyses. Together, these three characterization techniques reveal a coherent structural evolution pathway. Under the synergistic influence of microwave irradiation and pre-oxidation, the carbon framework gradually transforms from partially ordered graphite microcrystals to disordered amorphous carbon. Notably, in YYH-250W, the expansion of d_{002}, reduction of L_a, decrease in I_{D1}/I_G, and a simultaneous peak in free radical concentration indicates that the microcrystalline carbon has been deconstructed to a critical activation state.

Furthermore, Fourier-transform infrared (FTIR) spectroscopy was employed to analyze the surface chemical structures of activated carbon samples prepared under different microwave power densities, to elucidate the effect of microwave regulation on the evolution of surface functional groups, as shown in Fig. 5f. The FTIR spectra can be divided into four characteristic absorption regions: 3,600–3,000 cm^{-1}, corresponding to hydroxyl (–OH) stretching vibrations, 3,000–2,700 cm^{-1}, associated mainly with aliphatic hydrocarbons ($–CH_3$, $–CH_2$) vibrations, 1,800–1,000 cm^{-1}, representing various oxygen-containing functional groups (e.g., carbonyl C=O, ester C–O–C, and carboxyl groups), and 900–700 cm^{-1}, attributed to aromatic ring skeletal vibrations indicative of aromatic carbon structures[33].

Distinct differences in the surface functional composition among the six samples reveal that both microwave power and pre-oxidation significantly influence the reconstruction of surface chemistry. All samples display pronounced $–CH_3$/$–CH_2$ (aliphatic), and =CH (aromatic) vibration peaks around 2,900 cm^{-1} and below 3,000 cm^{-1}, confirming the coexistence of aliphatic hydrocarbons and aromatic carbon layers within the coal-based carbon framework[31]. In the THM series, strong carbonyl (C=O, ~1,700 cm^{-1}), and carboxyl-related peaks are observed at low power (200 W), indicating that the unoxidized coal retains abundant oxygen-containing groups such as carboxylic acids and ketones under mild treatment. As the power increases to 250 and 300 W, the intensity of the C=O-related peaks rapidly diminishes or even vanishes, suggesting that higher power induces more severe pyrolysis, resulting in the removal, cleavage, or condensation of oxygenated groups, and promoting deoxygenation and aromatization of the carbon framework.

Table 2 Physicochemical structural parameters of ACs

Sample	I_{D1}/I_G	L_a (nm)	L_c (nm)	d_{002} (nm)	$I_{peak,EPR}$
THM-200	2.83	4.43	0.94	0.38	67,021
THM-250	2.82	3.40	1.00	0.35	17,736
THM-300	2.50	3.49	0.95	0.38	5,006
YYH-200	3.24	4.15	1.03	0.37	41,825
YYH-250	2.61	3.06	0.92	0.39	23,152
YYH-300	3.08	3.51	0.97	0.38	8,117

In contrast, the YYH series (pre-oxidized samples) exhibits no distinct C=O absorption peak in its FTIR spectra but displays a strong hydroxyl (O–H) vibration near 3,400 cm^{-1}. Combined with the enhanced C–O absorption in the 1,200–1,000 cm^{-1} region, this indicates that pre-oxidation promotes the transformation of carboxyl and carbonyl groups into phenolic and ether-like structures, thereby improving the hydrophilicity and thermal stability of the carbon materials. This transformation may also stabilize the hydroxyl signal through hydrogen bond formation.

To further elucidate the influence of different microwave powers and pre-oxidation treatments on the surface chemical properties of coal-based activated carbons, X-ray photoelectron spectroscopy (XPS) was employed to systematically analyze the elemental composition, and functional group structures of the prepared samples[34]. The survey spectra (Supplementary Fig. S7) indicate that all samples primarily contain C, O, and N elements, exhibiting clear heteroatom-doping characteristics.

The core purpose of peak fitting is to resolve shifts in binding energy within the core levels (e.g., C 1s, O 1s, and N 1s) corresponding to different chemical environments, thus enabling precise identification of characteristic functional groups such as C=O, C–O, C–N, pyridinic N (N-6), and pyrrolic N (N-5)[18]. The results reveal that both microwave power and pre-oxidation treatment significantly affect the bonding configurations and relative contents of heteroatoms (N and O), thereby modulating the surface electronic environment and distribution of active sites in the carbon framework. These variations directly influence the strength of interactions between activated carbon and gas molecules such as CO_2, ultimately determining its adsorption performance and selectivity. Accordingly, the XPS peak-fitting spectra (Supplementary Fig. S8) not only provide direct evidence for the doping mechanisms of heteroatoms within the carbon lattice but also offer essential theoretical insight into the structure–property relationship between surface functional group regulation and adsorption behavior. Thus, XPS serves as a crucial analytical tool for probing the microstructural evolution of functionalized porous carbon materials[35].

The THM and YYH series samples exhibited pronounced differences in the elemental composition of C, O, and N, reflecting the distinct structural effects of microwave power and pre-oxidation treatment. In the THM series, as the microwave power increased from 200 to 300 W, the nitrogen content slightly decreased from 4.12 at.% to 3.67 at.%, while the oxygen content declined more significantly from 12.47 at.% to 8.03 at.%. This trend indicates that high-power microwave irradiation induces thermal decomposition or desorption of N- and O-containing functional groups, consistent with the disappearance of the C=O peak and the attenuation of C–O absorption bands observed in FTIR spectra.

In contrast, the YYH series samples, subjected to pre-oxidation, demonstrated a notable enhancement in heteroatom incorporation. The nitrogen content increased from 7.36 at.% to 10.06 at.%, markedly higher than that of the THM counterparts, while the oxygen content remained above 10 at.% (as demonstrated in Fig. 5g

& h). These results suggest that the synergistic effect of pre-oxidation and microwave treatment effectively promotes co-doping of nitrogen and oxygen, thereby enhancing the surface polarity and chemical reactivity of the carbon materials. The detailed quantitative data on nitrogen- and oxygen-containing functional groups for all activated carbon samples are summarized in Table 3.

As shown in Table 3, and the functional group distribution diagrams of activated carbons (Fig. 5i, k), distinct trends are observed in the surface chemical compositions. In the THM series, the dominant oxygen-containing groups are C=O and C–O species, with the proportion of C=O gradually decreasing as microwave power increases, confirming the thermal instability of carboxyl and carbonyl functionalities under high-energy conditions[24]. In contrast, the YYH series exhibits a generally higher C=O content, suggesting that the pre-oxidation treatment promotes the enrichment of oxidized fragments. Meanwhile, the lower proportion of C–O bonds implies that certain hydroxyl groups may have been converted into carbonyl structures or further aromatized.

Regarding nitrogen functionalities, four main types are identified: pyridinic-N (N-6), pyrrolic-N (N-5), graphitic-N (N-Q), and oxidized-N (N-O). In the THM series, N-6 and N-5 species are relatively scarce and dispersed. Conversely, the YYH series maintains a stable combined proportion of N-6 and N-5 above 5%, with particularly high concentrations in YYH-250W and YYH-300W (N-6 = 4.29%, N-5 = 2.72%). This indicates that pre-oxidation facilitates heteroatom incorporation at edge and vacancy sites, forming stable p-type dopant configurations. Such findings are consistent with the enhanced EPR defect signals, confirming that the synergistic effect of microwave irradiation and pre-oxidation provides preferential pathways for nitrogen doping at defect-rich locations.

In summary, the synergistic effect of pre-oxidation and microwave treatment effectively promotes nitrogen–oxygen co-doping, thereby enhancing the surface polarity and density of chemically active sites in the activated carbons. The nitrogen species are predominantly composed of pyridinic-N and pyrrolic-N, both of which exhibit strong electron-donating capability and high CO_2 affinity, providing a favorable structural foundation for subsequent adsorption enhancement. Compared with the untreated THM series, the YYH series not only maintains a higher nitrogen content but also demonstrates a more rational distribution of surface functional groups. This indicates that the combined pre-oxidation and microwave approach is an effective strategy for constructing highly polar and defect-enriched carbon frameworks, serving as a key route toward nitrogen–oxygen functionalization.

To further investigate the differences between the THM and YYH experimental groups, changes in surface oxygen-containing functional groups during the pre-oxidation process were examined. XPS and FTIR analyses were conducted on the raw coal samples THM and YYH. Supplementary Table S5 lists the elemental compositions of the two samples determined by XPS analysis. Supplementary Fig. S9 displays the peak patterns of oxygen functional groups in the XPS spectra, while Supplementary Fig. S10 presents the FTIR spectra. The results consistently reveal that pre-oxidation markedly increases the abundance and stability of oxygen-containing functional groups in YYH. Compared with THM, YYH exhibits higher O1s content and a significantly increased proportion of thermally stable C=O groups, accompanied by the depletion of aliphatic C–H structures and reconstruction of the aromatic framework. These results demonstrate that pre-oxidation transforms unstable moieties into polar carbonyl functionalities, providing a favorable structural basis for efficient microwave energy coupling and subsequent reaction activation. Consequently, this leads to the pronounced differences in physicochemical properties observed in the aforementioned samples.

CO_2 adsorption characteristics

Furthermore, CO_2 adsorption experiments were conducted to evaluate the adsorption performance of the synthesized activated carbons. Figure 6a presents the CO_2 adsorption isotherms at low temperature, while Fig. 6b shows those measured at ambient temperature. Evidently, the CO_2 adsorption capacity of the activated carbons increases with the enhancement of pore volume (V_{micro} and V_{total}), and nitrogen content. The CO_2 uptake at low temperature follows the order: YYH-250W > YYH-300W > YYH-200W > THM-300W > THM-250W > THM-200W. Whereas at ambient temperature, the order is YYH-250W > THM-300W > YYH-300W > YYH-200W > THM-250W > THM-200W. These trends indicate that ultramicropore volume primarily governs CO_2 adsorption capacity, while pore size distribution and the contents of nitrogen and oxygen functional groups also exert significant influence. Notably, YYH-300W possesses a V_{micro} that is 91.3% of that of THM-300W, yet exhibits a higher CO_2 adsorption capacity, further confirming the crucial role of N/O co-doping in CO_2 capture. Moreover, although YYH-300W exhibits smaller S_{BET}, V_{micro}, and V_{total} values compared with YYH-200W, its CO_2 uptake is superior, which can be attributed to its higher nitrogen content (10.06 at.%), suggesting that nitrogen functionalities significantly enhance CO_2 affinity.

Meanwhile, the influence of pore size distribution can be further elucidated by calculating the fraction of ultramicropores filled with CO_2. As shown in Fig. 6c and Table 4, the f_{CO_2} values of all samples increase progressively as the pore width expands from approximately 0.45 to 0.75 nm, exhibiting a distinct linear growth trend. This observation indicates that ultramicropores, particularly those within the range of 0.5–0.7 nm, play a crucial role in CO_2 adsorption. The trend correlates well with the molecular kinetic diameter of CO_2 (≈ 0.33 nm) and the strong wall interactions within narrow pores, demonstrating that precise regulation of pore size can substantially enhance selective adsorption performance.

In comparison across different samples, THM-200W exhibits the highest f_{CO_2} values throughout, indicating that its pore size distribution is more concentrated within the effective CO_2 filling range, thereby exhibiting higher pore utilization efficiency[34]. However, this sample does not achieve the highest overall CO_2 uptake, suggesting a limitation in total pore volume or available surface active sites. In contrast, YYH-300W shows slightly lower f_{CO_2} values

Table 3 Nitrogen and oxygen functional group contents of ACs

Sample	C1s (at.%)	O1s (at.%)	N1s (at.%)	C=O (at.%)	C–O (at.%)	N-6 (at.%)	N-5 (at.%)	N-Q (at.%)	N-O (at.%)
THM-200	83.41	12.47	4.12	5.3	6.59	1.22	1.52	0.9	0.48
THM-250	84.47	11.18	4.34	4.58	5.71	0.97	1.75	1.29	0.33
THM-300	88.3	8.03	3.67	3.76	3.26	0.94	1.08	1.08	0.56
YYH-200	80.69	11.95	7.36	6.78	4.43	2.49	2.87	1.07	0.93
YYH-250	80.55	10.8	8.65	6.3	3.84	3.19	2.72	2.08	0.66
YYH-300	80.81	10.25	10.06	5.92	3.29	4.29	2.72	2.04	1.01

https://doi.org/10.48130/scm-0026-0001

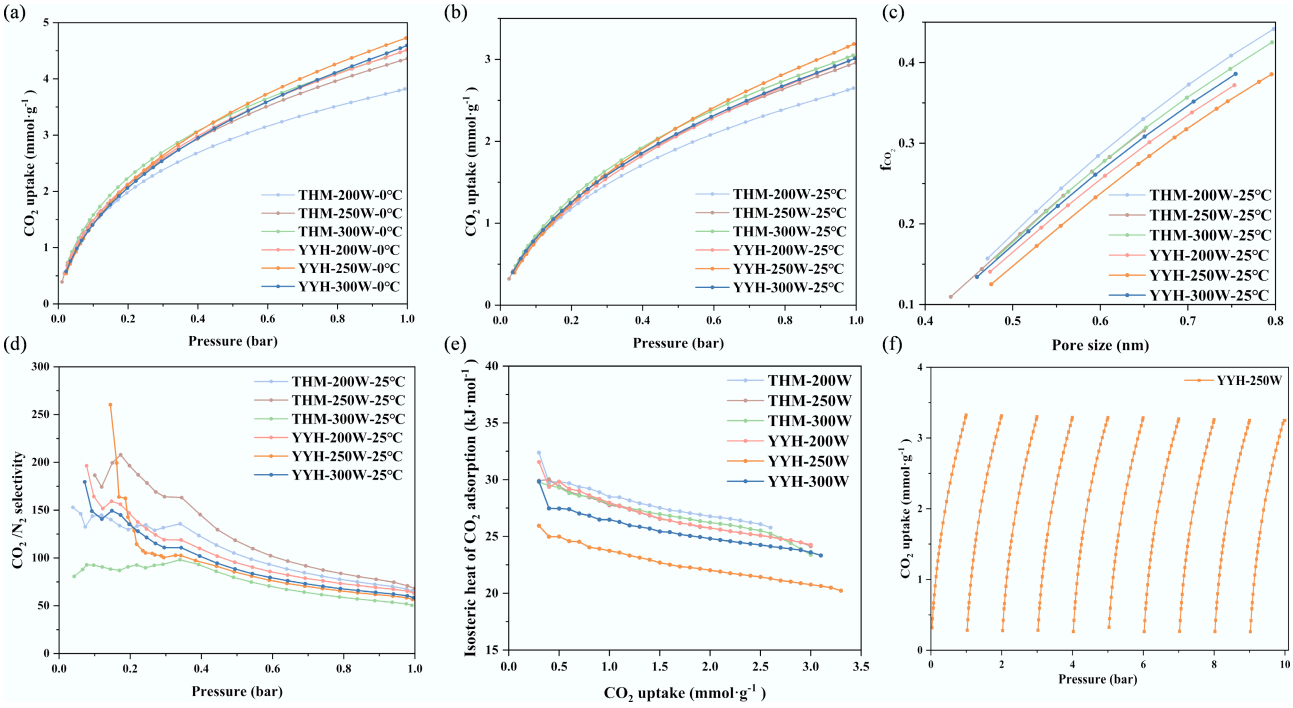

Fig. 6 The adsorption characteristics of CO_2. CO_2 adsorption isotherms at (**a**) 0 °C, and (**b**) 25 °C, (**c**) the fraction of micropore filling by CO_2 (f_{CO_2}), (**d**) the CO_2/N_2 selectivity at 25 °C and 0–1 bar (the CO_2/N_2 concentration ratio is 15:85); (**e**) The isosteric heat of CO_2 adsorption; (**f**) cycle adsorption curve of the sample YYH-250.

but significantly higher total CO_2 adsorption capacity, implying that its superior performance arises not only from favorable pore size matching but also from its larger pore volume, enhanced surface polarity, and abundant nitrogen/oxygen functional groups. Therefore, the correlation between f_{CO_2} and pore width highlights the necessity of balancing 'pore size optimization', and 'surface chemical regulation' in material design, serving as a crucial indicator for assessing the structural adaptability of porous adsorbents.

According to the ideal adsorbed solution theory (IAST), the calculated CO_2/N_2 selectivity (S_{ads}) decreases with increasing pressure, as illustrated in Fig. 6d[18]. All six samples exhibit S_{ads} values greater than 50, further confirming the excellent CO_2/N_2 adsorption selectivity of N/O co-doped activated carbons. These results indicate that the simultaneous optimization of pore structure and surface chemistry is an effective strategy for designing high-performance CO_2 adsorbents.

Figure 6e reveals the Qst-q curves of the samples. The results indicate that the Qst value gradually decreases with increasing adsorption load, revealing the energy heterogeneity of the adsorption sites. The relatively high initial Qst value demonstrates the adsorbent's strong affinity for CO_2 at low coverage. Concurrently, the representative sample YYH-250W exhibits the lowest adsorption heat. Meanwhile, Fig. 6f demonstrates the sample's excellent cycling performance, retaining 97.6% adsorption efficiency after ten cycles.

Table 4 CO_2 adsorption characteristics of ACs

Sample	CO_2/0 °C	CO_2/25 °C	N_2/25 °C	f_{CO_2}	CO_2/N_2 selectivity (1 bar)
THM-200	3.82	2.65	0.23	0.37	65
THM-250	4.36	2.96	0.25	0.36	68
THM-300	4.37	3.05	0.34	0.36	50
YYH-200	4.51	3.01	0.27	0.34	63
YYH-250	4.72	3.33	0.32	0.32	57
YYH-300	4.59	3.01	0.29	0.35	58

Conclusions

This work proposes a coupled strategy based on pre-oxidation pretreatment and microwave activation to efficiently construct nitrogen-doped ultramicroporous coal-based activated carbons, offering a new approach for multiscale structural synergy and optimization of gas adsorption performance. The detailed results are as follows:

(1) Benefiting from the high microwave absorption efficiency and volumetric heating characteristics, the activation time was significantly reduced to within 10 min. With increasing microwave power, both the specific surface area (up to 1,131 $m^2 \cdot g^{-1}$), and the proportion of ultramicropores increased markedly. Among all samples, YYH-250W exhibited the most optimized pore structure (V_{total} = 0.55 $cm^3 \cdot g^{-1}$).

(2) Microwave activation increased the defect density and surface active sites of the carbon framework, while pre-oxidation promoted synergistic N/O co-doping. The nitrogen content in the YYH series increased from 7.36 at.% to 10.06 at.%, with a targeted enhancement in pyridinic-N and pyrrolic-N proportions, forming electron-rich adsorption centers. Oxygen species mainly existed in C=O and C–O configurations, improving surface polarity.

(3) The YYH-250W sample exhibited the best CO_2 adsorption performance, achieving a CO_2 uptake of 4.72 $mmol \cdot g^{-1}$ at 0 °C and 1 bar, and maintaining 3.33 $mmol \cdot g^{-1}$ at 25 °C, with a CO_2/N_2 selectivity exceeding 50. The superior performance can be attributed to the synergistic effect of 0.6–0.7 nm ultramicropores and high N/O content, which collectively enhance CO_2 affinity and adsorption capacity.

Overall, the results demonstrate that coupling microwave activation with pre-oxidation pretreatment enables simultaneous

optimization of pore architecture and surface chemistry, yielding coal-based activated carbons with high selectivity and outstanding CO_2 capture performance.

Supplementary information

It accompanies this paper at: https://doi.org/10.48130/scm-0026-0001.

Author contributions

The authors confirm their contributions to the paper as follows: Yulin Feng: conceptualization, data curation, validation, writing – original draft; Xiaoxiao Meng: supervision, conceptualization, writing – review & editing; Jingyu Li: conceptualization, visualization, data curation; Naiyuan Xue: investigation; Wanjing Li: software; Miaoting Sun: software; Jiaxiang Chen: visualization; Xingxing Wang: data curation; Ruida Zhou: investigation; Wenjun Zhuang: methodology; Jihui Gao: project administration; Guangbo Zhao: funding acquisition; Wei Zhou: project administration. All authors reviewed the results and approved the final version of the manuscript.

Data availability

The datasets used or analyzed during the current study are available from the corresponding authors upon reasonable requests.

Funding

This work was financially supported by the National Natural Science Foundation of China (Grant No. U21A2062).

Declarations

Competing interests

The authors declare that they have no known competing financial interests or personal relationships that could have appeared to influence the work reported in this paper.

Author details

[1]School of Energy Science and Engineering, Harbin Institute of Technology, Harbin 150001, China; [2]CHN ENERGY Yuedian Taishan Power Generation Co., Ltd., Taishan 529200, China

References

[1] Joppa L, Willmott E. 2025. Six roadblocks to net zero — and how to get around them. *Nature* 640:31–34

[2] Shi M, Gao S, Lyu H, Ma Q, Zhang X, et al. 2024. Comparison on the development and policy frameworks of CCUS technology in China and the United States. *Clean Coal Technology* 30(10):19–31 (in Chinese)

[3] Yao Y, Lyu H, Peng X, Zhang X, Wang Y. 2024. Development trends and technological frontiers of global carbon management. *Clean Coal Technology* 30(10):32–40 (in Chinese)

[4] Matter JM, Stute M, Snæbjörnsdottir SÓ, Oelkers EH, Gislason SR, et al. 2016. Rapid carbon mineralization for permanent disposal of anthropogenic carbon dioxide emissions. *Science* 352:1312–1314

[5] Yang X, Wan Y, Zheng Y, He F, Yu Z, et al. 2019. Surface functional groups of carbon-based adsorbents and their roles in the removal of heavy metals from aqueous solutions: a critical review. *Chemical Engineering Journal* 366:608–621

[6] Chen W, Gong M, Li K, Xia M, Chen Z, et al. 2020. Insight into KOH activation mechanism during biomass pyrolysis: chemical reactions between O-containing groups and KOH. *Applied Energy* 278:115730

[7] Li T, An X, Fu D. 2023. Review on nitrogen-doped porous carbon materials for CO2 adsorption and separation: recent advances and outlook. *Energy & Fuels* 37(12):8160–8179

[8] Eichler JE, Leonard H, Yang EK, Smith LA, Lauro SN, et al. 2024. Dual-cation activation of N-enriched porous carbons improves control of CO_2 and N_2 adsorption thermodynamics for selective CO_2 capture. *Advanced Functional Materials* 34:2410171

[9] Hayat A, Sohail M, Alzahrani AYA, Ali H, Abu-Dief AM, et al. 2025. Recent advances in heteroatom-doped/hierarchical porous carbon materials: synthesis, design and potential applications. *Progress in Materials Science* 150:101408

[10] Wu J, Chen W, Chen L, Jiang X. 2022. Super-high N-doping promoted formation of sulfur radicals for continuous catalytic oxidation of H_2S over biomass derived activated carbon. *Journal of Hazardous Materials* 424:127648

[11] Luo J, Chen Y, Huang H, Ma R, Ma N, et al. 2023. Microwave-coordinated KOH directionally modulated N/O co-doped porous biochar from Enteromorpha and its structure–effect relationships in efficient CO_2 capture. *Chemical Engineering Journal* 473:145279

[12] Ren L, Wang F, Cheng F, Yang F, Zhang K. 2023. Mechanisms of gas generation from conventional and microwave pyrolysis of coal slime. *Chemical Engineering Journal* 452:139388

[13] Huang Q, Wei K, Xia H. 2019. Investigations in the recrystallization of evolved gases from pyrolysis process of melamine. *Journal of Thermal Analysis and Calorimetry* 138:3897–3903

[14] Shao J, Wang Y, Che M, Xiao Q, Demir M, et al. 2025. N, S Co-doped porous carbons from coconut shell for selective CO_2 adsorption. *Journal of the Energy Institute* 123:102273

[15] Wang J, Yin Y, Liu X, Liu Y, Xiao Q, et al. 2025. Potassium metaborate-activated boron-doped porous carbons for selective CO_2 adsorption. *Separation and Purification Technology* 376:134079

[16] Wang J, Wang Y, Liu X, Xiao Q, Demir M, et al. 2025. The synthesis of B-doped porous carbons via a sodium metaborate tetrahydrate activating agent: a novel approach for CO_2 adsorption. *Molecules* 30:2564

[17] Li J, Zhou W, Meng X, Huang Y, Li X, et al. 2024. Scalable confined-space microwave heating strategy enables the rapid preparation of N/O co-doped activated carbons with high gas capture capacity. *Carbon* 225:119152

[18] Tang Z, Gao J, Zhang Y, Du Q, Feng D, et al. 2023. Ultra-microporous biochar-based carbon adsorbents by a facile chemical activation strategy for high-performance CO_2 adsorption. *Fuel Processing Technology* 241:107613

[19] Mozaffari Majd M, Kordzadeh-Kermani V, Ghalandari V, Askari A, Sillanpää M. 2022. Adsorption isotherm models: a comprehensive and systematic review (2010–2020). *Science of The Total Environment* 812:151334

[20] Yuan J, Wang Y, Tang M, Hao X, Liu J, et al. 2023. Preparation of N, O co-doped carbon nanotubes and activated carbon composites with hierarchical porous structure for CO_2 adsorption by coal pyrolysis. *Fuel* 333:126465

[21] Durán-Jiménez G, Stevens LA, Kostas ET, Hernández-Montoya V, Robinson JP, et al. 2020. Rapid, simple and sustainable synthesis of ultra-microporous carbons with high performance for CO_2 uptake, via microwave heating. *Chemical Engineering Journal* 388:124309

[22] Li Y, Wang S, Liu H, Meng F, Ma H, et al. 2014. Preparation and characterization of melamine/formaldehyde/polyethylene glycol crosslinking copolymers as solid–solid phase change materials. *Solar Energy Materials and Solar Cells* 127:92–97

[23] Li J, Zhou W, Huang Y, Zhao Y, Li X, et al. 2024. Rapid, simple and sustainable preparation of N-rich activated carbons with high performance for gas adsorption, via microwave heating. *Separation and Purification Technology* 330:125464

[24] Zhu Y, Wu J, Zhang Y, Miao Z, Niu Y, et al. 2024. Preparation of hierarchically porous carbon ash composite material from fine slag of coal gasification and ash slag of biomass combustion for CO_2 capture. *Separation and Purification Technology* 330:125452

[25] Li J, Zhou W, Su Y, Zhao Y, Zhang W, et al. 2022. The enhancement mechanism of the microwave-assisted toluene desorption for activated carbon regeneration based on the constructive interference. *Journal of Cleaner Production* 378:134542

[26] Ghosh S, Sevilla M, Fuertes AB, Andreoli E, Ho J, et al. 2016. Defining a performance map of porous carbon sorbents for high-pressure carbon dioxide uptake and carbon dioxide–methane selectivity. *Journal of Materials Chemistry A* 4:14739−14751

[27] Wang X, Chen Q, Zhu H, Chen X, Yu G. 2023. *In-situ* study on structure evolution and gasification reactivity of biomass char with K and Ca catalysts at carbon dioxide atmosphere. *Carbon Resources Conversion* 6:27−33

[28] Taluja Y, SanthiBhushan B, Yadav S, Srivastava A. 2016. Defect and functionalized graphene for supercapacitor electrodes. *Superlattices and Microstructures* 98:306−315

[29] Chang CW, Kao YH, Shen PH, Kang PC, Wang CY. 2020. Nanoconfinement of metal oxide MgO and ZnO in zeolitic imidazolate framework ZIF-8 for CO_2 adsorption and regeneration. *Journal of Hazardous Materials* 400:122974

[30] Liu S, Zhang Y, Tuo K, Wang L, Chen G. 2018. Structure, electrical conductivity, and dielectric properties of semi-coke derived from microwave-pyrolyzed low-rank coal. *Fuel Processing Technology* 178:139−147

[31] Li H, Shi S, Lin B, Lu J, Ye Q, et al. 2019. Effects of microwave-assisted pyrolysis on the microstructure of bituminous coals. *Energy* 187:115986

[32] Pachfule P, Balan BK, Kurungot S, Banerjee R. 2012. One-dimensional confinement of a nanosized metal organic framework in carbon nanofibers for improved gas adsorption. *Chemical Communications* 48(14):2009−2011

[33] Chen Y, Kanan MW. 2025. Thermal Ca^{2+}/Mg^{2+} exchange reactions to synthesize CO_2 removal materials. *Nature* 638:972−979

[34] Iyer GM, Ku CE, Zhang C. 2025. Hyperselective carbon membranes for precise high-temperature H_2 and CO_2 separation. *Science Advances* 11:eadt7512

[35] Wan J, Zhang G, Jin H, Wu J, Zhang N, et al. 2022. Microwave-assisted synthesis of well-defined nitrogen doping configuration with high centrality in carbon to identify the active sites for electrochemical hydrogen peroxide production. *Carbon* 191:340−349